Applied Physics A (2019) 125:96
https://doi.org/10.1007/s00339-019-2384-4

Applied Physics A
Materials Science & Processing

Enhancement in photocatalytic performance of Ag–AgCl decorated with h-WO_3 and mechanism insight

Chen Chai[1] · Jianxin Liu[1] · Yawen Wang[1] · Xiaochao Zhang[1] · Donghong Duan[1] · Caimei Fan[1] · Yunfang Wang[1]

Received: 27 September 2018 / Accepted: 4 January 2019 / Published online: 11 January 2019

Abstract
A h-WO_3 decorated Ag–AgCl composite was prepared through facile precipitation and photoreduction methods and demonstrated to be a highly efficient and stable photocatalyst for the degradation of Rhodamine B (RhB) under visible light. Ag–AgCl/h-WO_3 exhibited much improved photocatalytic performance was elucidated from the physical–chemical properties of AgCl and h-WO_3 and the surface plasmon resonance effect of the Ag particles. The techniques of X-ray diffraction (XRD), field emission scanning electron microscopy (FESEM), X-ray photoelectron spectrometry (XPS) and photocurrent were used to characterize crystalline phases, morphology, composition and separation efficiency between electrons (e^-) and holes (h^+) of the synthesized composite photocatalyst. XPS results confirmed the existence of W^{5+} and W^{6+} on the surface of h-WO_3 sample, which favored electrons transfer between AgCl and Ag, and generated superoxide radical for the degradation of RhB. The active species trapping experiments results further demonstrated that the formation of superoxide radical during the system. Finally, the underlying photocatalytic mechanism for the removal of RhB by Ag–AgCl/h-WO_3 composite was examined.

1 Introduction

With the advance of society, environment and energy problems have become increasingly prominent, and photocatalyst based on efficient solar energy utilization has received more and more attention [1]. TiO_2 has been widely studied as the most representative traditional photocatalyst in the field of photocatalysis, but the large band gap (3.2 eV) restrains its practical application in visible light [2–5]. Therefore, doping or modifying TiO_2 with various elements has been a research hotspot for researchers in recent decades. Among them, due to the surface plasmon resonance (SPR) effect of the noble metal nanoparticles, the absorption of the photocatalyst in the visible light region can be improved, and more researchers have begun to introduce plasmon resonance materials into the field of photocatalysis. Typical plasmon resonance photocatalyst include Ag/TiO_2, Au/TiO_2, Pt/TiO_2 and so on [6–11].

In recent years, a series of comparative studies have been conducted for Ag/AgX (X = Cl, Br, I) plasmon resonance photocatalyst [12–14]; among all of these, Ag/AgCl photocatalyst has exhibited much more SPR effect of Ag nanoparticles and efficient photocatalytic performance under visible light [15–18]. In addition, as mentioned in the literature, the plasmon resonance effect between silver and silver chloride increased with the increase of silver content on the surface of the catalyst [19]. However, in some cases, various photocatalysts have drawbacks. For AgCl photocatalyst, on the one hand, the conduction band (CB) position of AgCl is lower than E ($O_2/\cdot O_2^-$) (− 0.33 eV vs. NHE), which means that AgCl has poor reduction ability to reduce oxygen to superoxide radical ($\cdot O_2^-$) [20]. On the other hand, the photocorrosion is also one of its main defects. Therefore, it is necessary and highly required to explore new visible-respond photocatalyst. As well known, WO_3 is an attractive choice due to its suitable band gap (~2.7 eV), environmental friendliness, low cost and good electron mobility, which can combine with silver chloride very well [21, 22]. Especially, a metastable hexagonal phase WO_3 (h-WO_3), which can promote the electron transfer on the conduction band of weakly reducing semiconductor materials by the circulatory system between valence tungsten (W^{5+} and W^{6+}), and can convert these electrons through the circulation into active species to enhance the photocatalytic activity of the material. Therefore, h-WO_3

✉ Yunfang Wang
wyfwyf53540708@163.com

[1] Department of Chemical Engineering, Taiyuan University of Technology, Taiyuan 030024, People's Republic of China

was selected to modify Ag–AgCl to further improve its photocatalytic performance.

In this paper, we synthesized a metastable hexagonal phase WO_3 (h-WO_3) by hydrothermal method. A novel Ag–AgCl decorated with h-WO_3 photocatalyst was prepared by simple precipitation method. And the prepared h-WO_3 with the low-valence state of tungsten was helpful to improve the reduction capacity of photoelectrons of AgCl and inhabited the photocorrosion of AgCl. To improve the SPR effect of AgCl/h-WO_3, silver particles were reduced on the surface of the catalyst. The photocatalytic activity and stability of the prepared samples were evaluated by the degradation efficiency of RhB under visible light ($\lambda > 420$ nm), and the prepared samples were characterized extensively to determine the material properties. The underlying photocatalytic mechanism was further discussed.

2 Experimental

2.1 Materials

All the reagents used were purchased by Sinopharm except that the tungstic acid reagent was purchased by Shanghai Aladdin. In addition, all reagents used in this study were of analytical grade purity and without further purified.

2.2 Materials preparation

2.2.1 Synthesis of h-WO_3

Typically, H_2WO_4 (6 mmol) was dissolved in 10 mL of hydrogen peroxide solution and vigorously stirred in a water bath. Then the above solution was heated up to 60 °C and obtained a pale green solution. Next, when the mixture was cooled to room temperature, hydrochloric acid (5 mL, 1 M), urea (4 mmol) and glycerol (2 mL) were added to the mixture in sequence. And then the ethanol was added to the above solution until the volume reached 30 mL. Subsequently, the as-obtained solution was transferred into a 50 mL Teflon–lined autoclave and kept at 180 °C for 12 h in an oven. After the autoclave was cooled to room temperature, the resulting black floccules were removed and washed with distilled water for 3 times, then dried in an oven at 60 °C for 12 h. And the preparation process is shown in Fig. 1a.

2.2.2 Synthesis of Ag–AgCl/h-WO_3 composite

Ag–AgCl/h-WO_3 composite was prepared via precipitation and photoreduction methods. In a typical experiment, h-WO_3 (0.2 g) and PVP (0.1 g) were dissolved into the mixed solution that consisted of 30 mL of water and 50 mL of anhydrous ethanol. And then $AgNO_3$ (3 g) was added to the above solution and vigorously stirred until $AgNO_3$ was completely dissolved. Hydrochloric acid (0.086 mL, 36 wt%) and sodium chloride (0.8775 g) were dispersed into 20 mL of distilled water and added dropwise to the above solution under tempestuously stirring. Then, it formed a milky white solution and was vigorously stirred for 24 h in dark. Next, the above solution was irradiated for 30 min with a 500 W Xenon lamp. And then the precipitation was collected by centrifugation, and washed with distilled water for 3 times. The obtained precipitation was dried in air at 60 °C for 8 h and Ag–AgCl/h-WO_3 was synthesized and recorded as AAW4.90. The preparation process is shown in Fig. 1b. Subsequently, a series of Ag–AgCl/h-WO_3 composite photocatalysts with different mass fractions of h-WO_3 were prepared in similar procedures, denoted as AAWx (x = 13.40, 9.35, 7.18, 5.83, 3.72 wt%). For comparison, Ag–AgCl photocatalyst was prepared without h-WO_3 and denoted as AA, AgCl/h-WO_3 photocatalyst was prepared without photoreduction process and labeled as AW4.90.

2.3 Characterization

The crystalline structure of the samples was characterized by XRD, which used a Rigaku D/max-2500 X-ray diffraction (Nippon Science) with a Cu Kα radiation operated at 40 kV and 30 mA. The morphologies and microstructures of the samples were observed with a FESEM (JSM-7001F). The element surface composition and the chemical state information of all samples were examined through XPS, which were measured on a 250 Xi X-ray photoelectron spectrometer (Thermo Fisher Scientific) with a micro focused monochromatic X-ray source (Al K_α) and the element binding energy was based on C 1s (284.8 eV).

2.4 Measurement of photocatalytic performance

The photocatalytic performances of the samples were evaluated by RhB degradation, which was performed on a Xenon lamp light source system with a 420 nm cut-off filter. First, 0.1 g photocatalyst was dispersed into 100 mL RhB (15 mg/L) aqueous solution, then it was magnetically stirred at room temperature in dark for 20 min to achieve adsorption and desorption equilibrium. Then the suspension was irradiated via Xenon lamp and took out 4.5 mL sample every 3 min. After finishing the reaction, all samples would be centrifuged and the concentration of RhB was measured via using an ultraviolet–visible spectrophotometer.

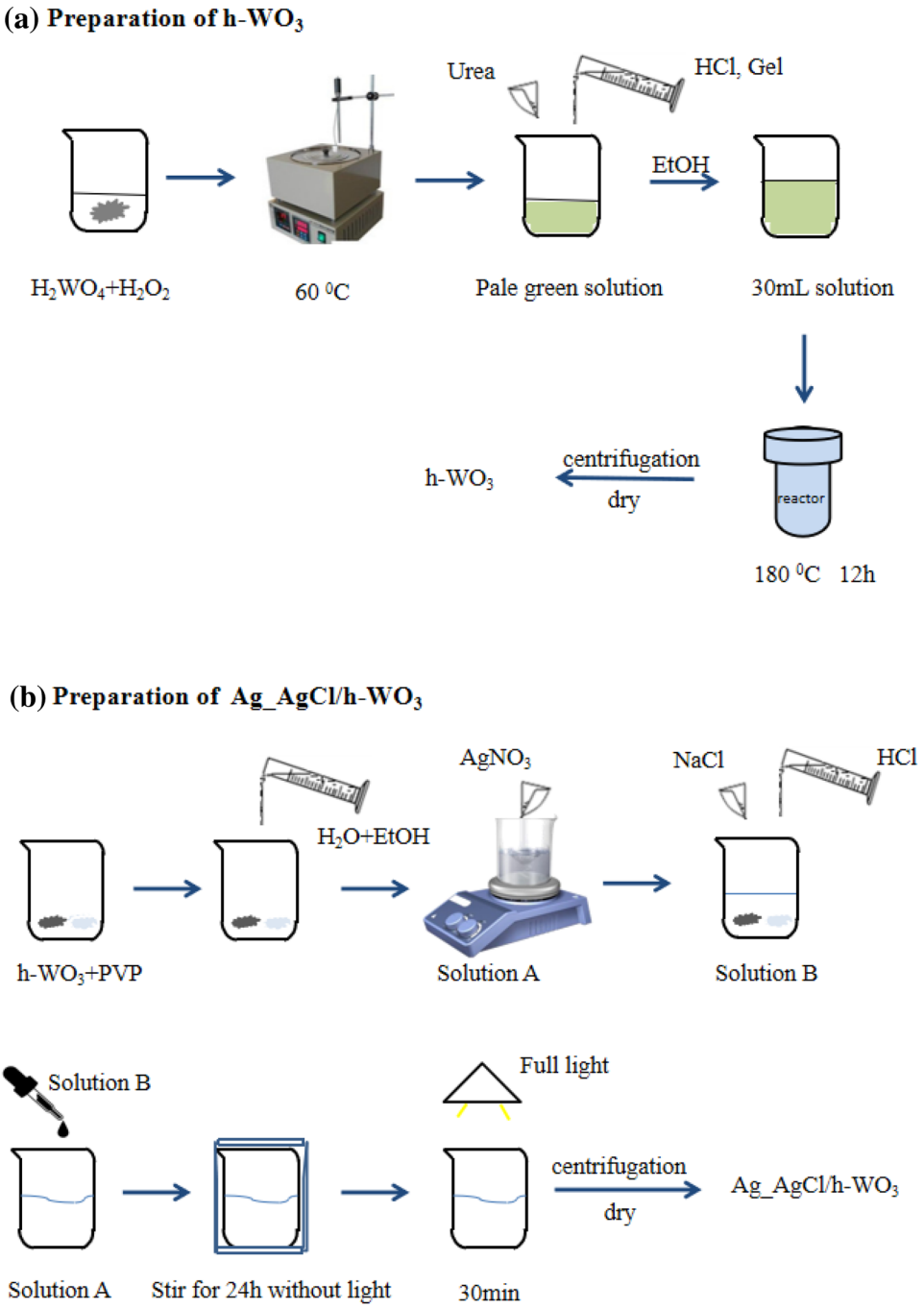

Fig. 1 Preparation flow charts of h-WO_3 (**a**) and AAW (**b**)

3 Results and discussion

3.1 Characterization of the prepared catalyst

The crystalline phases of all samples were identified by XRD, as shown in Fig. 2a. It can be seen that the diffraction peaks of the prepared h-WO_3 are well consistent with the phase of hexagonal (JCPDS no. 85-2459) [23]. The as-prepared AgCl shows five major diffraction peaks at 27.9°, 32.3°, 46.4°, 54.9°, and 57.7°, which correspond to the cubic AgCl (JCPDS no. 31-1238) [24]. In the XRD pattern of the prepared AW4.90, the diffraction peaks are in agreement with the characterized peaks of pure AgCl and no obvious peaks belong to h-WO_3, and this is due to low content of h-WO_3. In the XRD patterns of AAW hybrid photocatalysts with different mass ratios of h-WO_3, we cannot see the diffraction peaks of Ag^0 and h-WO_3, this may be attributed to the low mass ratio of Ag^0 and h-WO_3 and weak initial peak intensity, resulting in the deletion of Ag^0 and h-WO_3 diffraction peaks in XRD. To look into the diffraction peaks of Ag^0

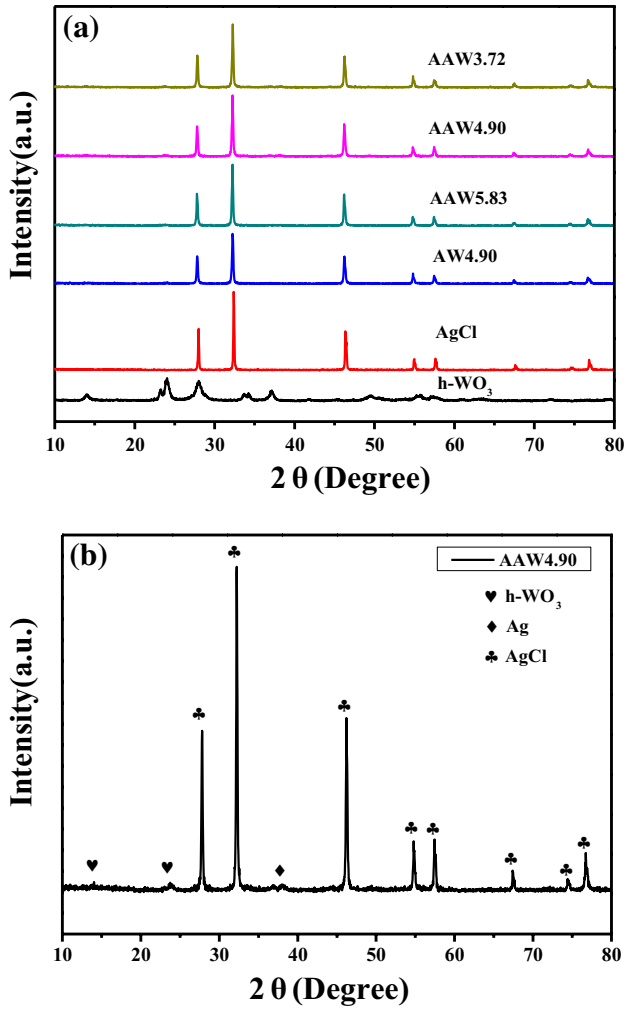

Fig. 2 XRD patterns of the as-prepared samples (**a**) and the enlarged AAW4.90 (**b**)

and h-WO_3, we enlarged the XRD pattern of AAW4.90, as shown in Fig. 2b. It can be found that there are two weak diffraction peaks of h-WO_3 at 14.0° and 23.8°, and a weak diffraction peak corresponds to Ag^0 (JCPDS no. 65-2871) at 38.1° [23, 24]. These characterization results indicate that AAW4.90 composite was successfully prepared.

The surface morphology of all samples has been further characterized by FESEM, as shown in Fig. 3. Figure 3a shows an irregular structure of h-WO_3 formed by many spherical particles clustered together and a magnified image of the spherical particle with an outer diameter of about 2–5 μm is shown in Fig. 3b. From Fig. 3c, d, we can see that AgCl is composed of many smooth irregular block structures. In Fig. 3e, the AA material are severely agglomerated together to form a large, rough surface block structure, compared with Fig. 3c, d; after enlarging the image, we can see that there are many particles about 500 nm clustered together on the surface of AgCl in Fig. 3f. As is shown in Fig. 3g, h, AA particles are well coated on the surface of h-WO_3 to form AAW4.90 composite. After h-WO_3 was added, the distribution of surface particles was more uniform than that of Fig. 3f, indicating that the presence of h-WO_3 could weaken the agglomeration of AA particles to some extent. From the perspective of the effect of morphology on the performance of photocatalyst, the homogeneous dispersion of AA particles on the surface of h-WO_3 can also promote the photocatalytic performance.

The typical survey scan XPS spectrum of AAW4.90 composite is shown in Fig. 4a, which manifests that the composite photocatalyst mainly contains Ag, Cl, W, O and C (in which the C element mainly comes from the instrument itself). Figure 4b represents the high-resolution XPS spectrum of W 4*f* in AAW4.90 photocatalyst. The two strong peaks emerged at 36.08 and 38.18 eV respectively correspond to W $4f_{7/2}$ and W $4f_{5/2}$ of W^{6+}, while the other two peaks observed at 35.21 and 37.26 eV are related to W $4f_{7/2}$ and W $4f_{5/2}$ of W^{5+} [25, 26]. The characterization result indicates that there are two valence states of tungsten element on the surface of AAW4.90 heterojunction photocatalyst. In Fig. 4c, O 1*s* spectrum of AAW4.90 could be well devolved into three obvious peaks. The peaks at 530.62 and 531.83 eV are attributed to the lattice oxygen of W–O bond and absorbed O_2 group, respectively [26, 27]. And the peak at 532.89 eV belongs to the OH^- group, which origins from absorbed water [28]. The peaks located at 367.36 and 373.35 eV belong to Ag $3d_{5/2}$ and Ag $3d_{3/2}$ of Ag^+, while those at 368.28 and 374.28 eV are attributed to Ag $3d_{5/2}$ and Ag $3d_{3/2}$ of Ag^0, respectively. In addition, the XPS results of Ag 3*d* spectrum support the existence of Ag^0 from Fig. 4d [28, 29]. In Fig. 4e, two peaks of Cl 2*p* exist at 197.64 and 199.30 eV, assigned to Cl $2p_{3/2}$ and Cl $2p_{1/2}$ of Cl^- [28].

3.2 Photocatalytic performance

Figure 5a shows Ag–AgCl with different mass ratios of h-WO_3 to degrade RhB under visible light. Among the six kinds of AAWx samples, AAW4.90 exhibited the most pronounced photocatalytic activity. As a result, there is an optimal ratio between h-WO_3 and Ag–AgCl, namely 4.90 wt%.

The photocatalytic activities of h-WO_3, AgCl, AA, AW4.90 and AAW4.90 were examined in terms of the degradation of RhB at room temperature under visible light irradiation, as shown in Fig. 5b. From the degradation result, 12% of RhB was degraded in 9 min by pure h-WO_3. Compared to pure AgCl, AA exhibited stronger photocatalytic activity, indicating that the reduction of Ag^0 in advance helps to further increase the activity of the plasmon resonance structure [30].

The activity of AW4.90 composite is higher than that of AgCl and AA materials, which indicates that an effective heterojunction structure was formed between AgCl

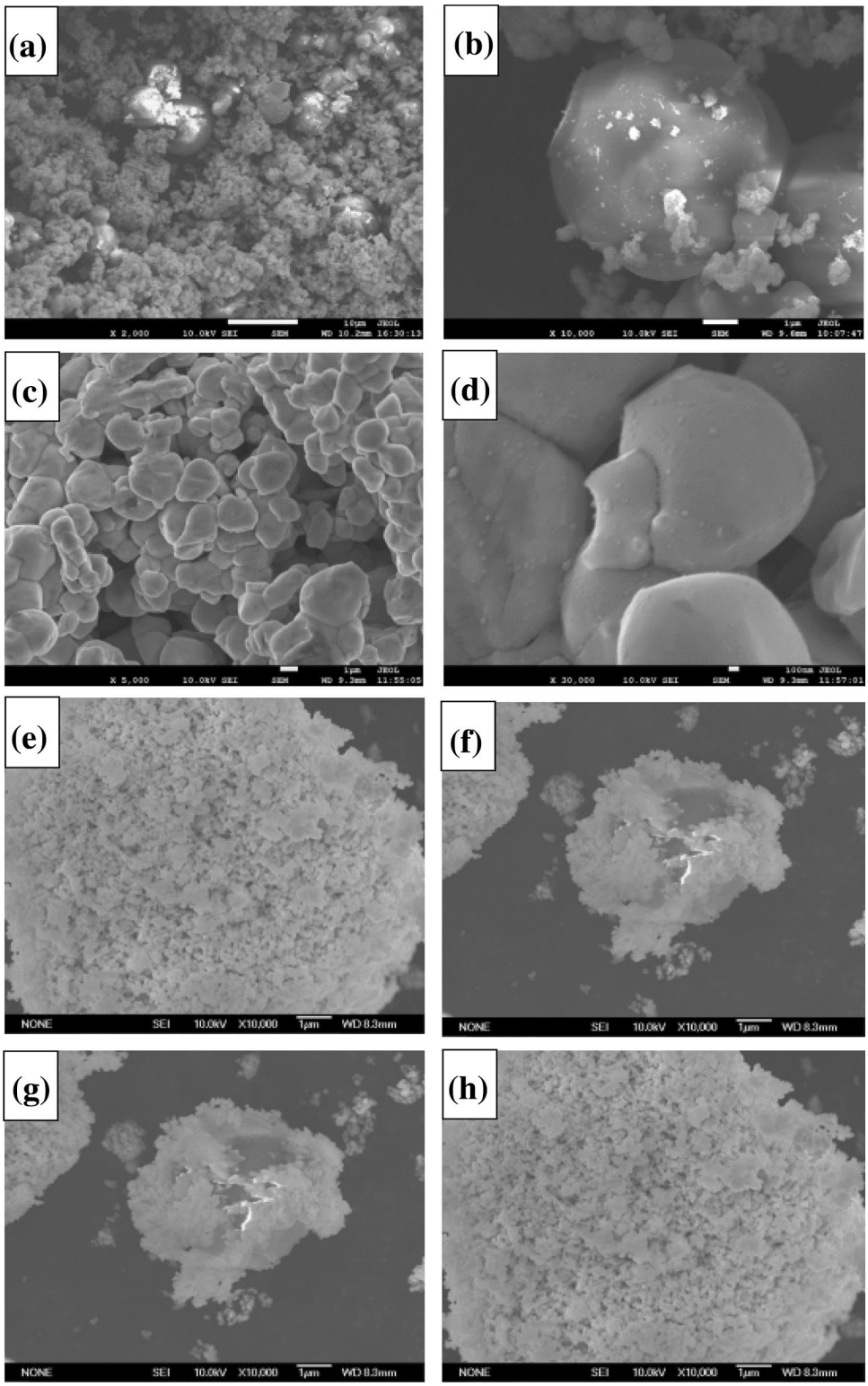

Fig. 3 SEM images of the prepared samples: **a, b** h-WO_3, **c, d** AgCl, **e, f** AA, **g, h** AAW4.90

and h-WO_3. However, compared with AW4.90 composite, AAW4.90 composite exhibited stronger photocatalytic performance, the degradation efficiency of AW4.90 and AAW4.90 for RhB are 86.7% and 99.6% within 9 min, respectively. This experimental result certifies that the Ag–AgCl plasmon resonance photocatalyst can form an effective heterojunction structure with h-WO_3, that is, the existence of h-WO_3 can effectively enhance the photocatalytic performance of the AA plasmon resonance system.

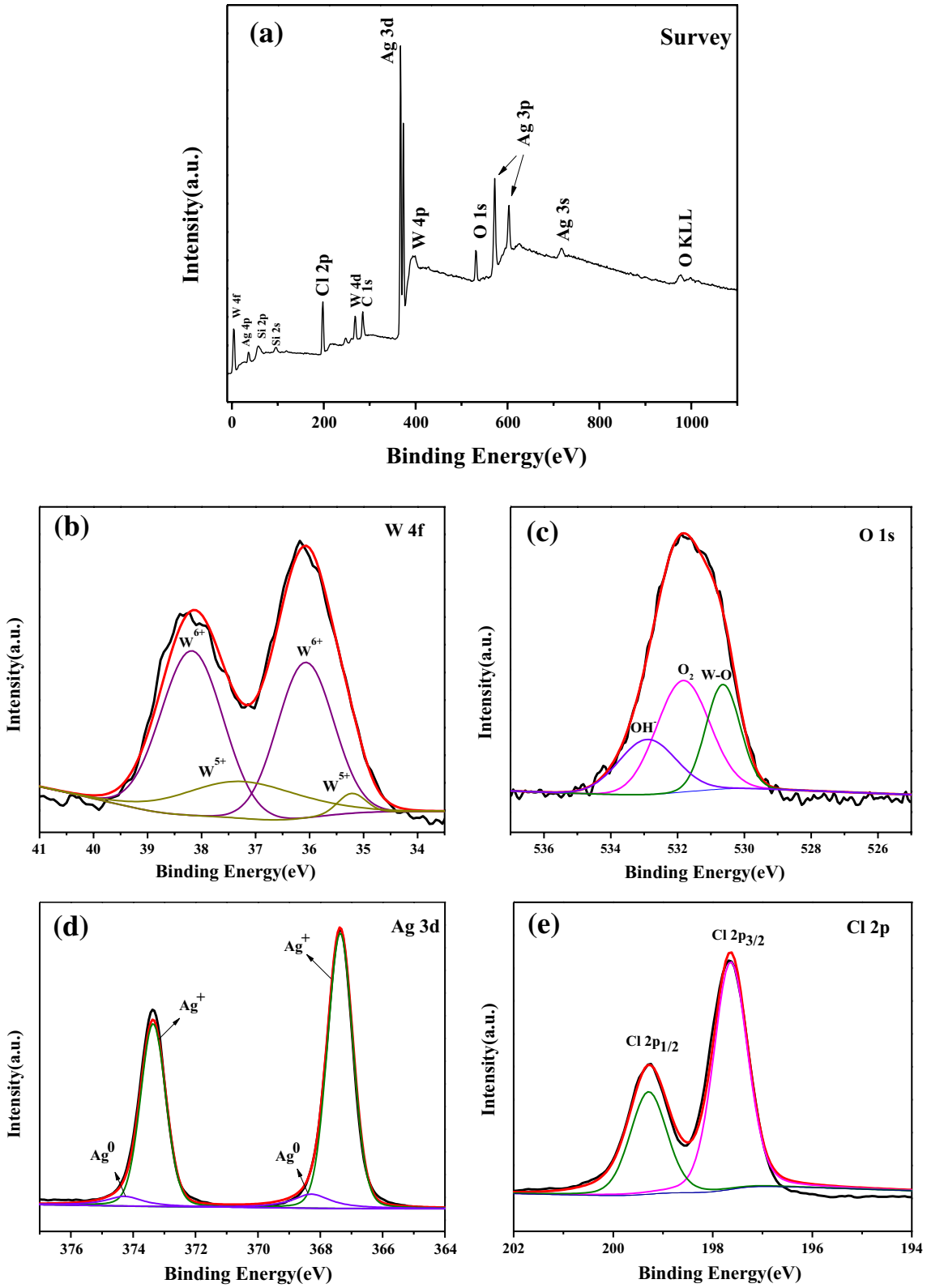

Fig. 4 XPS spectra of as-synthesized AAW4.90: **a** survey, **b** W 4*f*, **c** O 1*s*, **d** Ag 3*d*, **e** Cl 2*p*

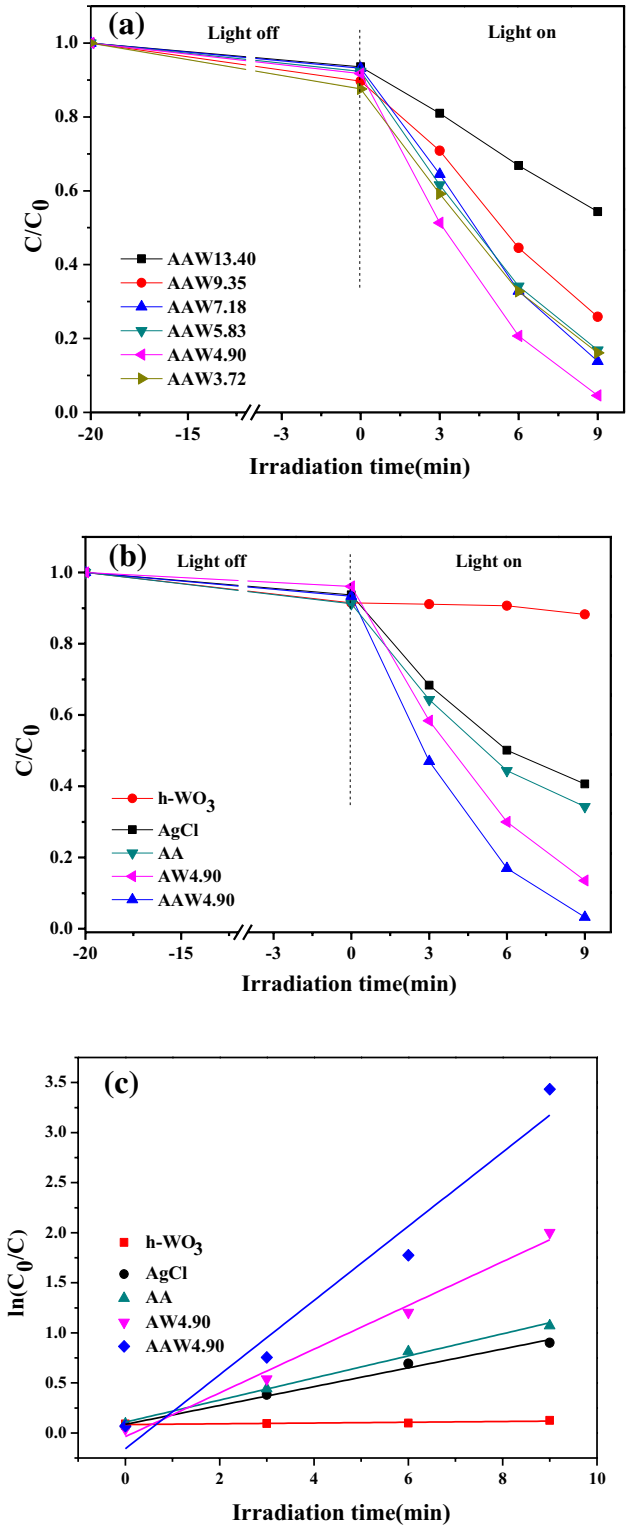

Fig. 5 **a** Degradation efficiency of RhB by AA with different mass ratio of h-WO_3; **b** plots C/C_0 for RhB in the presence of various photocatalysts; **c** kinetic curves for RhB degradation over the as-prepared photocatalysts

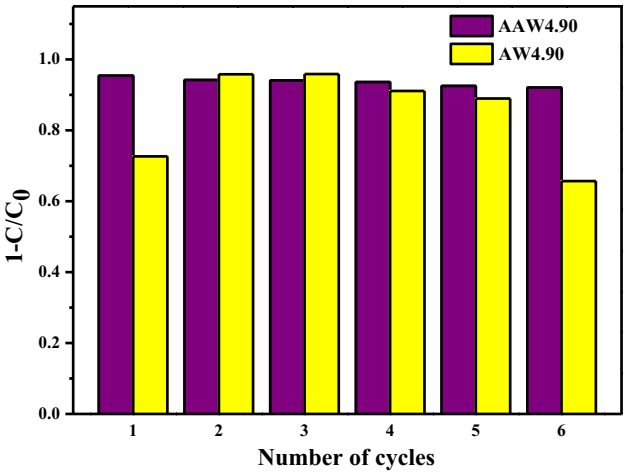

Fig. 6 The cycle tests of RhB degradation in the presence of AAW4.90 and AW4.90 under visible light irradiation

3.3 Photocatalytic stability of AAW4.90 and AW4.90 composite

As is well known, Ag-based photocatalysts are susceptible to be corroded under visible light irradiation, therefore, the stability test is another important index for evaluating Ag-based photocatalysts. In Fig. 6, the photocatalytic stabilities of AW4.90 and AAW4.90 were tested and compared. After six cycles, the photocatalytic degradation rate of AAW4.90 composite for RhB only decreases by 3%, for the reduction of the silver element in advance helps to enhance the stability and activity of the catalyst and to some extent overcomes the light corrosion. However, the photocatalytic stability of AW4.90 shows a trend of rising first and then decreasing. The photocatalytic degradation process can be speculated as follows: to begin with, the reduction amount of Ag^0 was relatively small due to the shorter time of photoreaction, therefore, the absorption of visible light by the plasmon resonance system was less, resulting in its low activity. In the subsequent cycles, since the system already had Ag^0 and formed a SPR effect, the photocatalytic activity was significantly improved and had a certain degree of stability. However, in the last cycle, AW4.90 showed a sharp decrease in the degradation rate of RhB, since the formation of more silver particles would envelop the catalyst, leading to a decrease in photocatalytic activity.

In addition, the release amount of Ag^+ in solution after six cycles of AAW4.90 and AW4.90 composite were analyzed by inductively coupled plasmon mass spectrometry (ICP). The test results are as follows: the Ag^+ emissions of AAW4.90 and AW4.90 composites were 49.238 mg/L and 59.358 mg/L, respectively. The test results demonstrate the inference of the difference in stability between the two heterojunction photocatalyst. After six cycles, due to the dual

effects of the instability and photocorrosion of the AW4.90 heterojunction photocatalytic system, a large amount of Ag^+ were precipitated in the system, leading to a decrease in photocatalytic activity of the sample.

3.4 Photocatalytic mechanism analysis

To have a deep understanding into the photocatalytic mechanism, a series of capture tests of active species were carried out. In these experiments, isopropanol (IPA), ammonium oxalate (AO) and *p*-benzoquinone (PBQ) were introduced as the scavengers of hole (h^+) and hydroxyl radical (·OH) and $\cdot O_2^-$, respectively. As shown in Fig. 7a, with the addition of AO and PBQ, the photocatalytic degradation rates of RhB were significantly inhibited, while the effect was negligible after addition of IPA. The results of the experiments confirmed that the main active species of AAW4.90 composite are $\cdot O_2^-$ and h^+.

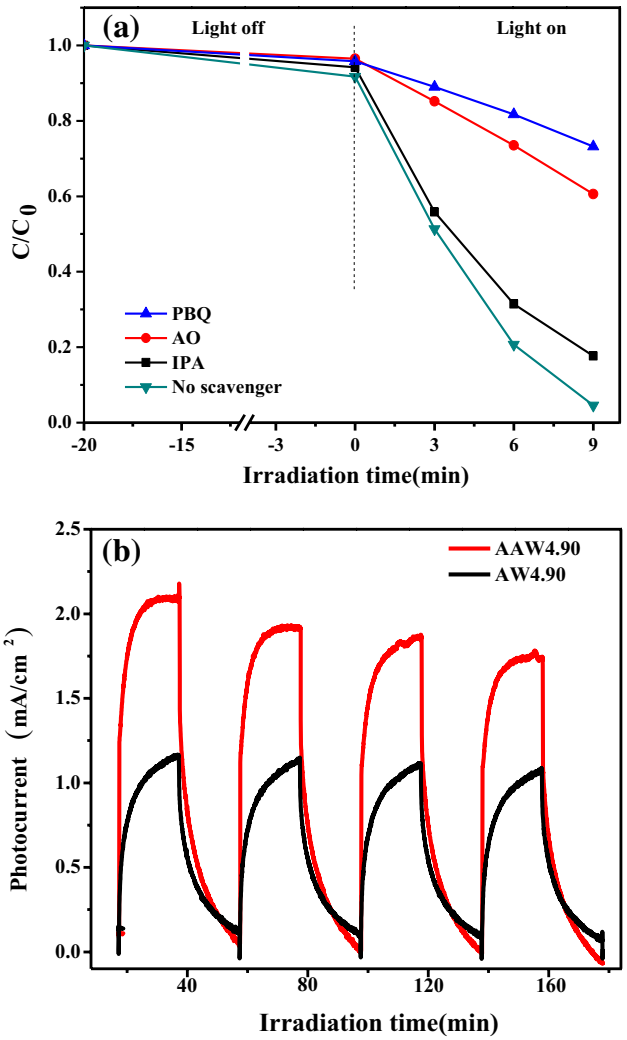

Fig. 7 Trapping experiments of active species over AAW4.90 (**a**), photoelectric conversion performances of AAW4.90 and AW4.90 (**b**)

In addition, the interface charge separation and transport of the photo-generated electrons and holes is an important factor for the photocatalytic properties. In this study, transient photocurrent responses were used to investigate the charge separation efficiency. The transient photocurrent responses for AAW4.90 and AW4.90 samples under visible light irradiation in an on-and-off cycle mode are shown in Fig. 7b. It is clearly seen that the photocurrent of AAW4.90 composite is higher than that of AW4.90 sample, which suggests the recombination of electron–hole (e^-–h^+) pairs is greatly inhibited and enhances their separation efficiency largely.

Based on the above results, the enhanced photocatalytic performance of AAW4.90 composite could be mainly attributed to the improved separation of photo-generated charge carriers. Therefore, the schematic energy band illustration of the heterojunction for AAW4.90 composite is shown in Fig. 8. The band gaps of the h-WO_3 and pure AgCl are 2.7 eV and 3.25 eV, and h-WO_3 can be excited by visible light, while pure AgCl cannot be excited by visible light. However, once Ag particles form the SPR effect on the surface of AgCl, Ag–AgCl composite can effectively absorb visible light.

The specific process of photocatalysis is described as follows: first, Ag–AgCl and h-WO_3 are excited by visible light to generate e^-–h^+ pairs, as in the formulas (1) and (2):

$$\text{Ag–AgCl} + h\nu \rightarrow \text{Ag–AgCl}\,(e^-) + \text{Ag–AgCl}\,(h^+), \quad (1)$$

$$\text{h-WO}_3 + h\nu \rightarrow \text{h-WO}_3(e^-) + \text{h-WO}_3(h^+). \quad (2)$$

Due to the formation of Ag^0, the SPR effect would be formed on the surface of AgCl sample. The CB of AgCl (− 0.093 eV) is more negative than that of h-WO_3 (+ 0.74 eV) and the valence band (VB) of h-WO_3 is more positive than that of AgCl. Considering the inner electric field and energy band structure, the photoexcited electrons on the CB of AgCl can rapidly transfer to the CB of h-WO_3, while the photo-generated holes on the VB of h-WO_3 can migrate to the VB of AgCl. As a result, the photo-generated e^-–h^+ pairs can be separated efficiently in the photocatalytic system of AAW4.90 heterojunction. At the same time, the h^+ accumulated on the VB of AgCl will combine with Cl^- in the system to form chlorine radical (Cl·) with strong oxidation ability, which can efficiently degrade RhB, as shown in the following formula (3):

$$\text{Cl}\cdot + \text{RhB} \rightarrow \text{Cl}^- + \text{Degradation product}. \quad (3)$$

According to the results of active species, h^+ and $\cdot O_2^-$ are the main active species in the RhB degradation with AAW4.90 composite. In AAW4.90 heterojunction

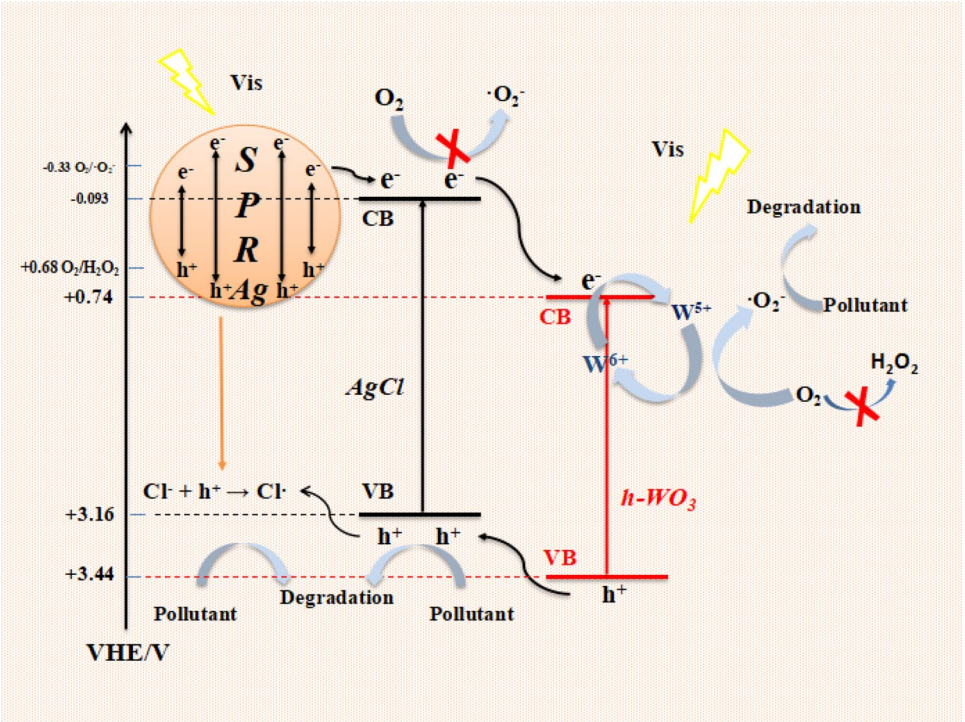

Fig. 8 The proposed photocatalytic mechanism diagram of AAW4.90 composites on the degradation of RhB under visible light irradiation

structure, the CB potentials of h-WO_3 (+0.74 eV) and AgCl (−0.093 eV) are more positive than the standard potential of $\cdot O_2^-$ [E ($O_2/\cdot O_2^-$) (−0.33 V vs NHE)], which means that neither the electrons on the h-WO_3 nor the electrons on the AgCl can combine with O_2 to form $\cdot O_2^-$. Therefore, how do $\cdot O_2^-$ come into being during photocatalytic process? According to the results of XPS analysis, W^{5+} and W^{6+} appeared on the surface of AAW4.90. And the low-valence tungsten present in the system can be excited by visible light ($\lambda > 420$ nm) and lose electrons to generate high-valence tungsten [31]. Therefore, we speculated the W^{5+} and W^{6+} are associated with the generation of $\cdot O_2^-$. In AAW4.90 heterojunction, W^{6+} is reduced to W^{5+} by the electrons on the CB of h-WO_3. At the same time, electrons generated by the excitation of W^{5+} by visible light have sufficient energy to reduce oxygen to produce $\cdot O_2^-$. Therefore, h^+, $\cdot O_2^-$ and Cl· active species generated during photocatalytic process can completely degrade RhB in the water.

4 Conclusions

In conclusion, the use of h-WO_3 decorated Ag–AgCl as an efficient photocatalyst for RhB degradation under visible light has been proved. When the mass of h-WO_3 reached 4.90%, Ag–AgCl/h-WO_3 can degrade RhB by 99.6% in 9 min under visible light. These superiorities could be accounted for the following reasons. First, the circulation of W^{5+}/W^{6+} is beneficial for electrons transfer between Ag–AgCl and h-WO_3 and produces $\cdot O_2^-$. Second, the decoration of h-WO_3 can prevent photocorrosion of AgCl, leading to better stability. Third, the surface plasmon resonance effect formed by the presence of elemental silver is more conducive to the efficient use of electrons.

Acknowledgements This work was financially supported by the Youth National Natural Science Foundation of China (no. 21808151 and no. 21506144).

References

1. X. Chen, S. Shen, L. Guo, S.S. Mao, Chem. Rev. **110**, 6503–6570 (2010)
2. A. Fujishima, K. Honda, Nature **238**, 37–38 (1972)
3. E. Borgarello, J. Kiwi, E. Pelizzetti, M. Visca, M. Grätzel, Nature **289**, 158–160 (1981)
4. J. Wang, F. Meng, W. Xie, C. Gao, Y. Zha, D. Liu, P. Wang, Appl. Phys. A Mater (2018) https://doi.org/10.1007/s00339-018-2027-1
5. J. Zhou, Y. Cheng, J. Yu, J. Photochem. Photobiol. A **223**, 82–87 (2011)
6. Z.Y. Jiang, X.H. Zhang, Z.M. Yuan, J.C. Chen, B.B. Huang, D.D. Dionysiou, G.H. Yang, Chem. Eng. J. **348**, 592–598 (2018)
7. D.B. Ingram, S. Linic, J. Am, Chem. Soc. **133**, 5202–5520 (2011)
8. J.L. Yang, C.Y. Mou, Appl. Catal. B Environ. **231**, 283–291 (2018)
9. S. Khore, S.R. Kadam, S.D. Naik, B.B. Kale, R. Sonawane, New J. Chem. **42**, 10958–10968 (2018)
10. A. Bora, K. Mohan, S. Doley, P. Goswami, S.K. Dolui, Catal. Sci. Technol. **8**, 4180–4192 (2018)
11. Y.T. Ma, Z.H. Li, Appl. Surf. Sci. **452**, 279–285 (2018)

12. R. Dong, B. Tian, C. Zeng, T. Li, T. Wang, J. Zhang, J. Phys. Chem. C **117**, 213–220 (2013)
13. C.H. An, S.T. Wang, Y.G. Sun, Q.H. Zhang, J. Zhang, C.Y. Wang, J.Y. Fang, J. Mater. Chem. A **4**, 4336–4352 (2016)
14. Y. Fan, W. Ma, D. Han, S. Gan, X. Dong, L. Niu, Adv. Mater. **27**, 3767–3773 (2015)
15. G.Q. Wang, H. Mitomo, Y. Matsuo, K. Niikura, K. Ljiro, J. Mater. Chem. B **1**, 5899–5907 (2013)
16. J.F. Guo, B.W. Ma, A.Y. Yin, K.N. Fan, W.L. Dai, J. Hazard. Mater. **211**, 77–82 (2012)
17. H. Zhang, X. Fan, X. Quan, S. Chen, H. Yu, Environ. Sci. Technol. **45**, 5731–5736 (2011)
18. J.J. Yu, D.P. Sun, T.H. Wang, F. Li, Chem. Eng. J. **334**, 225–236 (2018)
19. C.P. Byers, H. Zhang, D.F. Swearer, M. Yorulmaz, B.S. Hoener, D. Huang, A. Hoggard, W.S. Chang, P. Mulvaney, E. Ringe, N.J. Halas, P. Nordlander, S. Link, C.F. Landes, Sci. Adv. **1**, e1500988 (2015)
20. Y.Z. Hong, Y.H. Jiang, C.S. Li, W.Q. Fan, X. Yan, M. Yan, W.D. Shi, Appl. Catal. B Environ. **180**, 663–673 (2016)
21. Y. Liu, Y.H. Yang, Q. Liu, Y.M. Li, J. Lin, W.Z. Li, J. Li, J. Colloid Interface Sci. **512**, 86–95 (2018)
22. S.C. Wang, H.J. Chen, G.P. Gao, T. Butburee, M.Q. Lyu, S. Thaweesak, J.H. Yun, A.J. Du, G. Liu, L.Z. Wang, Nano Energy **24**, 94–102 (2016)
23. P.I. Gouma, K. Kalyanasundaram, J. Mater. Sci. **50**, 3517–3522 (2015)
24. X.X. Yao, X.H. Liu, J. Hazard Mater. **280**, 260–268 (2014)
25. Y.M. Ren, Q. X, X.L. Zheng, Y.Z. Fu, Z. Wang, H.L. Chen, Y.X. Weng, Y.C. Zhou, Appl. Catal. B Environ. **231**, 381–390 (2018)
26. L.W. Wang, J.X. Liu, Y.W. Wang, X.C. Zhang, D.H. Duan, C.M. Fan, Y.F. Wang, Colloids Surf. A **541**, 145–153 (2018)
27. M.L. Yin, L.M. Yu, S.Z. Liu, Mater. Lett. **186**, 66–69 (2017)
28. Q.Y. Li, G.R. Duan, J. Luo, X.H. Liu, J. Energy. Chem. **27**, 826–835 (2018)
29. H.B. Fang, X. Cao, J.J. Yu, X. Lv, N. Yang, T.H. Wang, W. Jiang, J. Mater. Sci. **54**, 286–301 (2019)
30. P. Wang, B.B. Huang, X.Y. Qin, X.Y. Zhang, Y. Dai, J.Y. Wei, M.H. Whangbo, Angew. Chem. Int. Ed. **47**, 7931–7933 (2008)
31. M. Yan, G. Li, C. Guo, W. Guo, D. Ding, S. Zhang, S. Liu, Nanoscale **8**, 17828–17835 (2016)